

AD706414



DAMAGE THRESHOLD STUDIES IN LASER CRYSTALS

By

Concetto R. Giuliano, Robert W. Hellwarth, LaVerne D. Hess, and
Gerald R. Rickel

HUGHES RESEARCH LABORATORIES
HUGHES AIRCRAFT COMPANY
3011 Malibu Canyon Road
Malibu, California 90265

Contract NO. F19628-69-C-0277
Project NO. 8693

SEMI-ANNUAL REPORT NO. 1
JANUARY 1970

This research was supported by the
Advanced Research Products Agency
under ARPA Order NO. 1434.



THIS DOCUMENT HAS BEEN APPROVED FOR PUBLIC
RELEASE AND SALE; ITS DISTRIBUTION IS UNLIMITED.

Contract Monitor: C. Martin Stickley
OPTICAL PHYSICS LABORATORY

Prepared for

AIR FORCE CAMBRIDGE RESEARCH LABORATORIES
OFFICE OF AEROSPACE RESEARCH
UNITED STATES AIR FORCE
BEDFORD, MASSACHUSETTS 01730

Reproduced by the
CLEARINGHOUSE
for Federal Scientific & Technical
Information Springfield Va. 22151

**BEST
AVAILABLE COPY**

**MISSING PAGE
NUMBERS ARE BLANK
AND WERE NOT
FILMED**

DAMAGE THRESHOLD STUDIES IN LASER CRYSTALS

Semiannual Technical Report No. 1

January 1970

This research was supported by the
Advanced Research Projects Agency of
The Department of Defense and was
monitored by
Air Force Cambridge Research Laboratories

ARPA Order Number:	1434
Program Code Number:	9D10
Name of Contractor:	Hughes Aircraft Company
Effective Date of Contract:	21 May 1969
Contract Expiration Date:	15 June 1970
Contract Number:	F19628-69-C-0277
Principal Investigator and Phone Number:	Concetto R. Giuliano (213)456-6411, Ext. 285
Project Scientist or Engineer and Phone Number:	Same as above
Short Title of Work:	Damage Threshold Studies
Amount of Contract:	\$159,925.00
Contract Monitor:	C. Martin Stickley
Contributors:	C.R. Giuliano R.W. Hellwarth L.D. Hess G.R. Rickel

HUGHES AIRCRAFT COMPANY
Research Laboratories Division
3011 Malibu Canyon Road
Malibu, California 90265

This document has been approved
for public release and sale; its
distribution is unlimited.

ABSTRACT

In this report a mode-controlled giant pulse laser oscillator and amplifier are described. The oscillator employs a temperature-controlled resonant reflector, a dye Q-switch laser and a 2 mm aperture to assure single mode operation. The result of preliminary threshold measurements on a few different ruby samples are presented. Equations which describe the propagation of the gaussian mode are examined in order to answer some important questions concerning focusing inside dielectric media. The potential usefulness of the scanning electron microscope as a tool for examining surface damage is pointed out by the presentation of a few interesting photomicrographs. The theoretical effort is concentrated on the effects of strong optical fields on relatively low densities of electrons in the conduction band of a transparent polar crystal. The present studies have led to agreement with the general opinion that these electrons are a key link in the optical pulse damage process. However, the present work indicates that significant electron heating above ambient lattice temperatures does not occur at the optical intensities in question. An entirely new role of the electrons in laser induced damage is suggested.

TABLE OF CONTENTS

I.	EXPERIMENTAL STUDIES ON OPTICAL DAMAGE	1
A.	Introduction and Summary of Results	1
B.	Experimental Apparatus	1
C.	Longitudinal Mode Selection	8
D.	Results of Threshold Experiments	11
E.	Definition of Threshold	12
F.	Electron Microscope Observations	13
G.	Mode Propagation Computations	17
H.	Plans for Next Period	21
II.	THEORETICAL STUDIES ON OPTICAL DAMAGE	23
A.	Introduction and Summary of Results	23
B.	Estimate of the Conditions for Crystal Rupture	24
C.	Calculation of Heating and Absorption by Conduction Electrons	25
D.	Plans for Next Period	29
	REFERENCES	31

LIST OF ILLUSTRATIONS

Fig. 1. Schematic representation of experimental apparatus 2

Fig. 2. Giant pulse ruby laser system 3

Fig. 3. Giant pulse ruby laser head 4

Fig. 4. Typical photo monitoring Fabry-Perot interferogram, near-field, and far-field beam patterns 6

Fig. 5. Ruby laser amplifier 7

Fig. 6. Temperature tuned resonant reflector 9

Fig. 7. Plot of percent transmission at 6328 Å of the resonant reflector versus temperature 10

Fig. 8. Scanning electron micrographs of the exit surface damage at different magnifications 14

I. EXPERIMENTAL STUDIES ON OPTICAL DAMAGE

A. Introduction and Summary of Results

The experimental effort during the reporting period has been devoted mainly to working toward obtaining reliable single mode operation of our ruby oscillator and sufficiently high power to exceed damage threshold in ruby and sapphire under mild focusing conditions. To these ends we have carried out a number of refinements on a giant pulse ruby laser which is essentially a copy of one described previously,¹ and have built an adequate ruby laser amplifier. The main modification in the oscillator is the installation of a temperature controlled resonant reflector which will give reliable longitudinal mode control. The resonant reflector used previously did not employ temperature control, and thermal drifting resulted in poor reliability in obtaining a single longitudinal mode. Calibration of the power monitoring detector has been accomplished by two independent means. Various time delay circuitry for the oscillator-amplifier combination has been built, installed, and demonstrated to perform reliably. Preliminary threshold measurements have been made on a few different samples so that some important comparisons could be made. We have examined equations which describe the propagation of the gaussian mode in order to answer some important questions concerning focusing inside dielectric media. The potential usefulness of the scanning electron microscope as a tool for examining surface damage is pointed out by the presentation of a few interesting photomicrographs. With the exception of the temperature controlled resonant reflector, which it is hoped will be available soon, we are in an excellent position to begin a variety of meaningful experiments.

B. Experimental Apparatus

The experimental setup is shown in Figs. 1 and 2. The laser head is shown in Fig. 3. The oscillator employs a 4 in. long x 1/4 in. diameter ruby which is pumped by two linear lamps in a double elliptical pump cavity. The ruby crystal is water-cooled by a closed-cycle refrigeration system maintained at 0°C. The high reflectivity mirror is coated with a 99+% reflectivity high field damage coating from Perkin Elmer Corporation. Q-switching is accomplished with a rotating

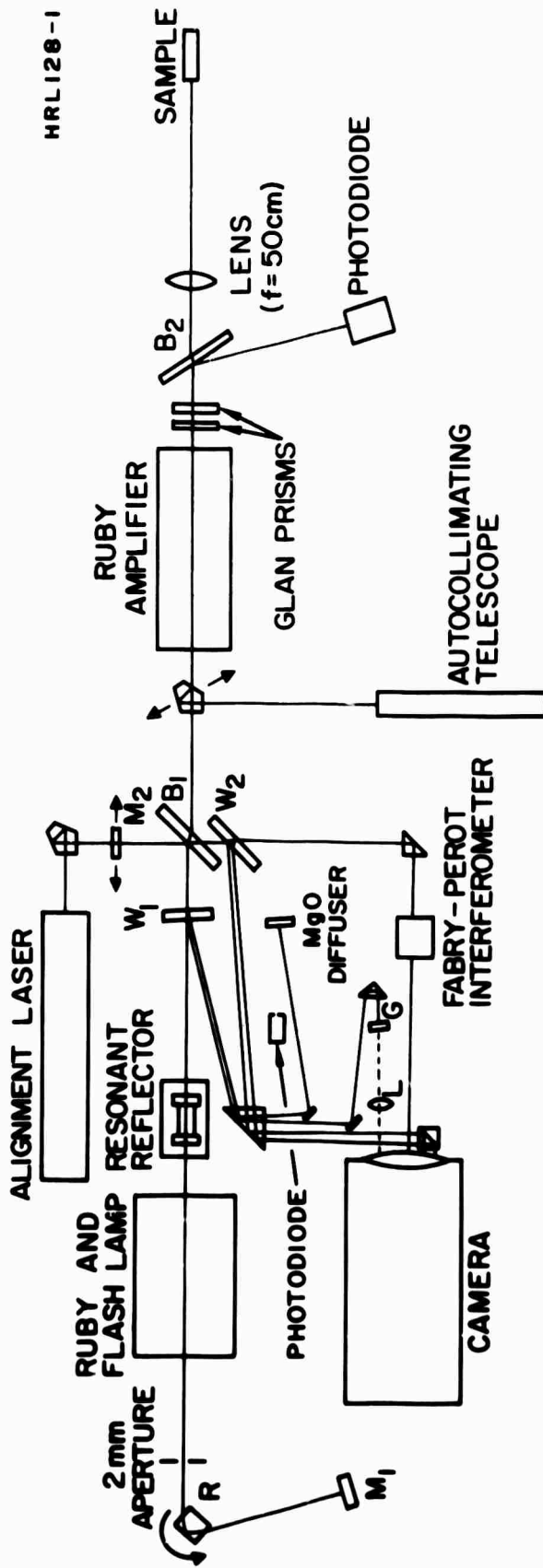


Fig. 1. Schematic representation of experimental apparatus.

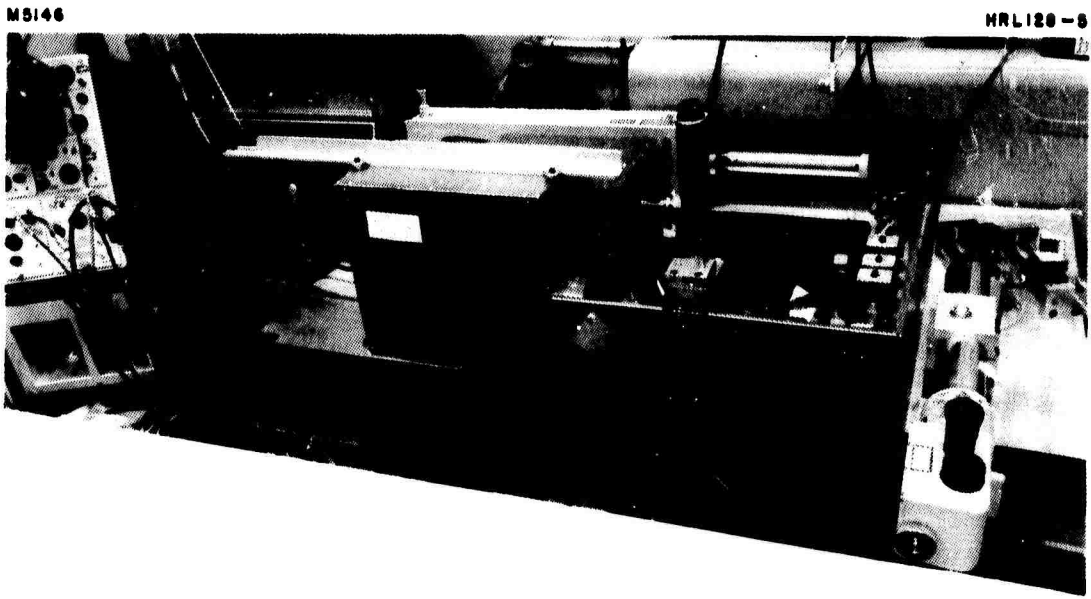


Fig. 2. Giant pulse ruby laser system.

M4787

0700 5

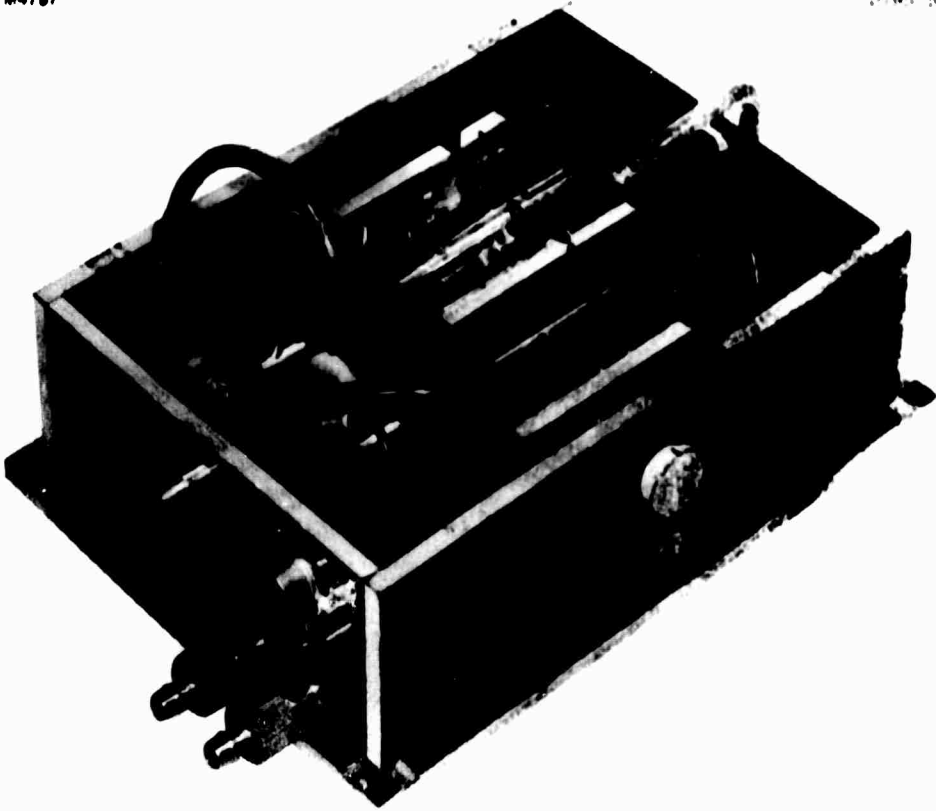


Fig. 3. Giant pulse ruby laser head.

cube prism placed such that the beam enters and leaves at Brewster's angle when the system is in alignment. The temperature controlled resonant reflector is described in more detail in the following section. Collimated light from the He-Ne alignment laser is used in conjunction with the auto-collimating telescope to align the various elements in the laser.

Portions of the laser beam are split off in various ways (see Fig. 1), so that the power output, near- and far-field patterns, and Fabry-Perot patterns can be monitored for each shot. This is accomplished in the following way. Light reflecting from wedged beamsplitter W_1 gives two diverging beams; one of them hits the magnesium oxide diffuser, where the scattered light is monitored by a biplanar photodiode used as our power monitor. The second beam from W_1 hits ground glass screen G , where it is photographed through lens L and the 1 m focal length camera focused at infinity. This gives a magnified ($\sim 5x$) near-field picture. Another portion of the light is removed by beamsplitter B_1 and hits mirror M_2 , which can be placed in or out of position depending on the use of the alignment laser. From M_2 the light either goes to the Fabry-Perot interferometer or can be partially reflected from wedged beamsplitter W_2 , where it results in a pair of far-field patterns. An example of the data is shown in Fig. 4. A 0.6 neutral density filter is placed near the focal plane of the camera so that the far-field pattern and the Fabry-Perot pattern can be seen at two different exposures. The two Glan prisms are used as a variable attenuator after the amplifier. Beamsplitter B_2 samples the light to the photodiode which monitors the power incident upon the focusing lens, which was designed for minimum spherical aberration (Special Optics). A photograph of the amplifier is shown in Fig. 5.

The water cooled amplifier ruby is 6 in. long x 0.5 in. diameter, with one end wedged relative to the other by about 0.5° . The input end of the amplifier rod is antireflection coated to minimize the chances of oscillation within the amplifier itself. The ruby rod is closely coupled to a helical flashlamp, which is pumped with a power supply capable of delivering 8 kJ in a 3 msec pulse. The power supply employs a pulse shaping network of 20 sections, each section pumping for 150 usec.

6967

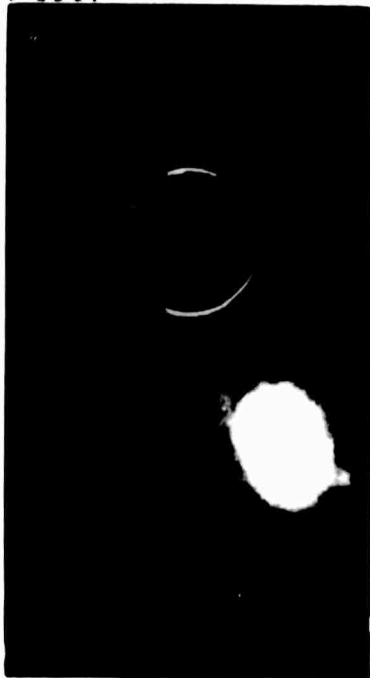


Fig. 4.
Typical photo monitoring Fabry-Perot
interferogram, near-field, and far-
field beam patterns. The difference
in optical density between the two
halves of the picture is N.D. 0.6.
The free spectral range of the inter-
ferometer is 1.6 cm^{-1} .

M 6975

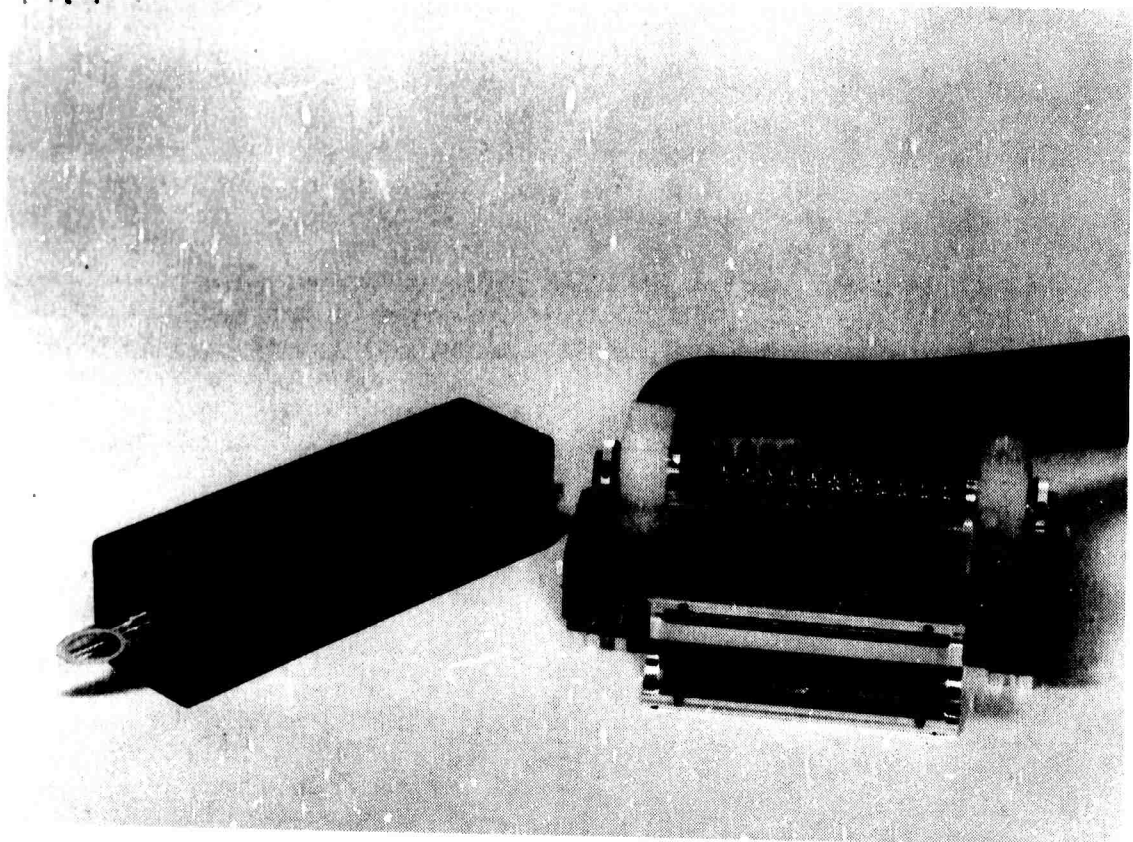


Fig. 5. Ruby laser amplifier.

C. Longitudinal Mode Selection

A multiple element resonant reflector has been designed to enhance longitudinal mode selection. The optical resonator and associated equipment for accurate temperature regulation of the system is shown in Fig. 6. The resonator consists of two quartz plates optically contacted to a quartz spacer with dimensions of 5.14, 3.42 and 3.00 mm, respectively. It is well known that except for extra modes in the regions of high loss, the general effect of the extra surfaces added to the laser cavity is to impose a modulation on the original modes. The frequency spacings of the plates are $2/3$ and 1 cm^{-1} . Thus, the combined effect of the two plates is to enhance cavity modes separated by 2 cm^{-1} and to discriminate against intermediate modes, while the surfaces separated by the spacer enhance modes separated by $1-2/3 \text{ cm}^{-1}$. A temperature change alters the optical length of the plates, but has little effect on the length controlled by the spacer because the temperature coefficient of expansion for quartz is an order of magnitude lower than the refractive index coefficient. Thus the device can be thermally tuned to bring all of the surfaces into resonance to provide a maximum reflectivity of 40% at the resonant frequency.

The optical transmission of light from a He-Ne laser through the resonant reflector at different temperatures is shown in Fig. 7. The bandwidth of this laser is small compared with that of any of the resonator spacings, and its output frequency does not necessarily correspond to a resonant frequency of the device; therefore, maximum reflectivity is not expected. Measurements of this type were made in order to gain information which would simplify application of the device to the pulsed ruby laser. The bandwidth of the ruby gain profile is large enough to include two resonances of the reflector system. Independent thermal control of the ruby and resonant reflector will be used to bring the system into resonance to provide optimum longitudinal mode selectivity.

The resonant reflector is not yet permanently incorporated in our system. This fact represents the major obstacle to our being completely ready to perform a number of desired damage threshold experiments. There have been a number of difficulties associated with the fabrication and installation of the resonant reflector, all of which can be summed up in the result that it will not stay together; i.e., the optical contacting has not been accomplished for a variety of reasons.

M 6974

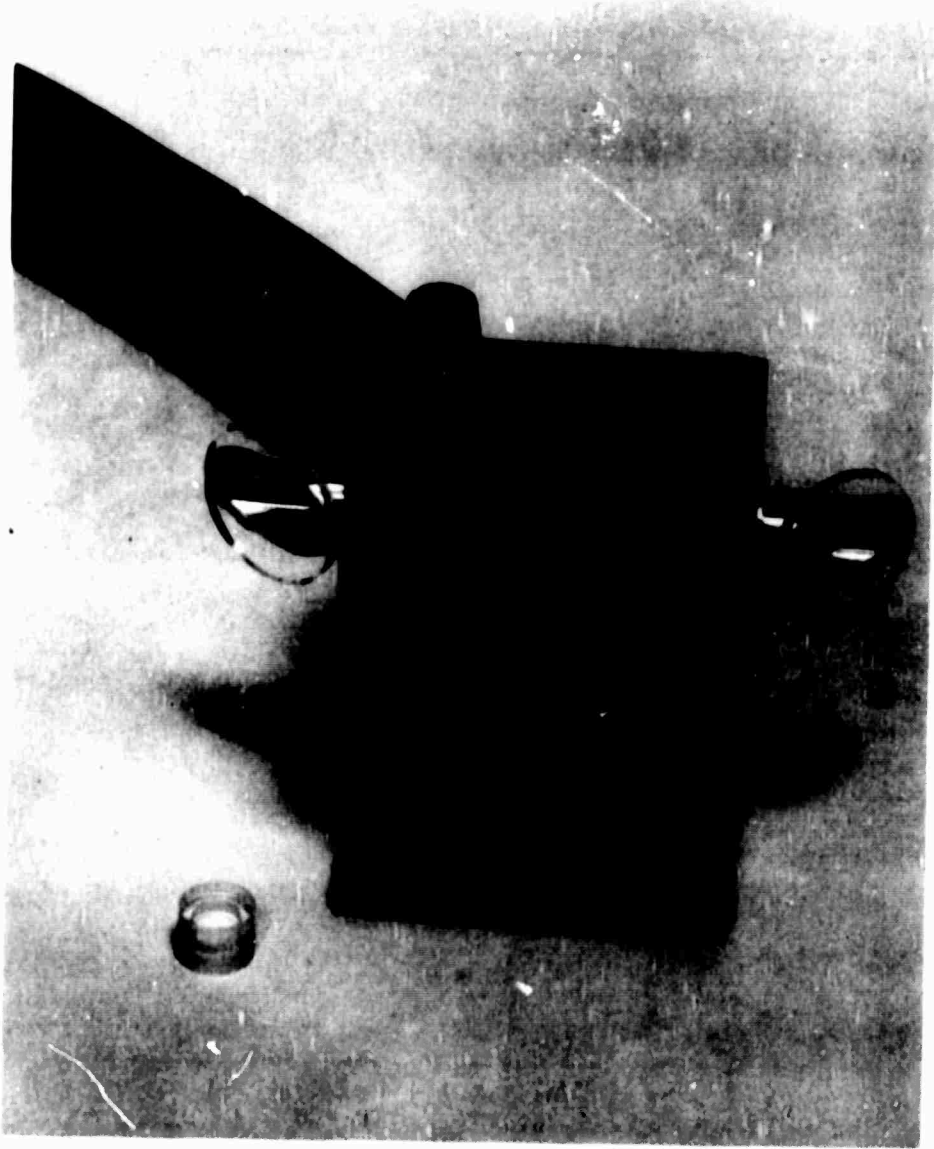


Fig. 6. Temperature tuned resonant reflector
(lower left) and housing.

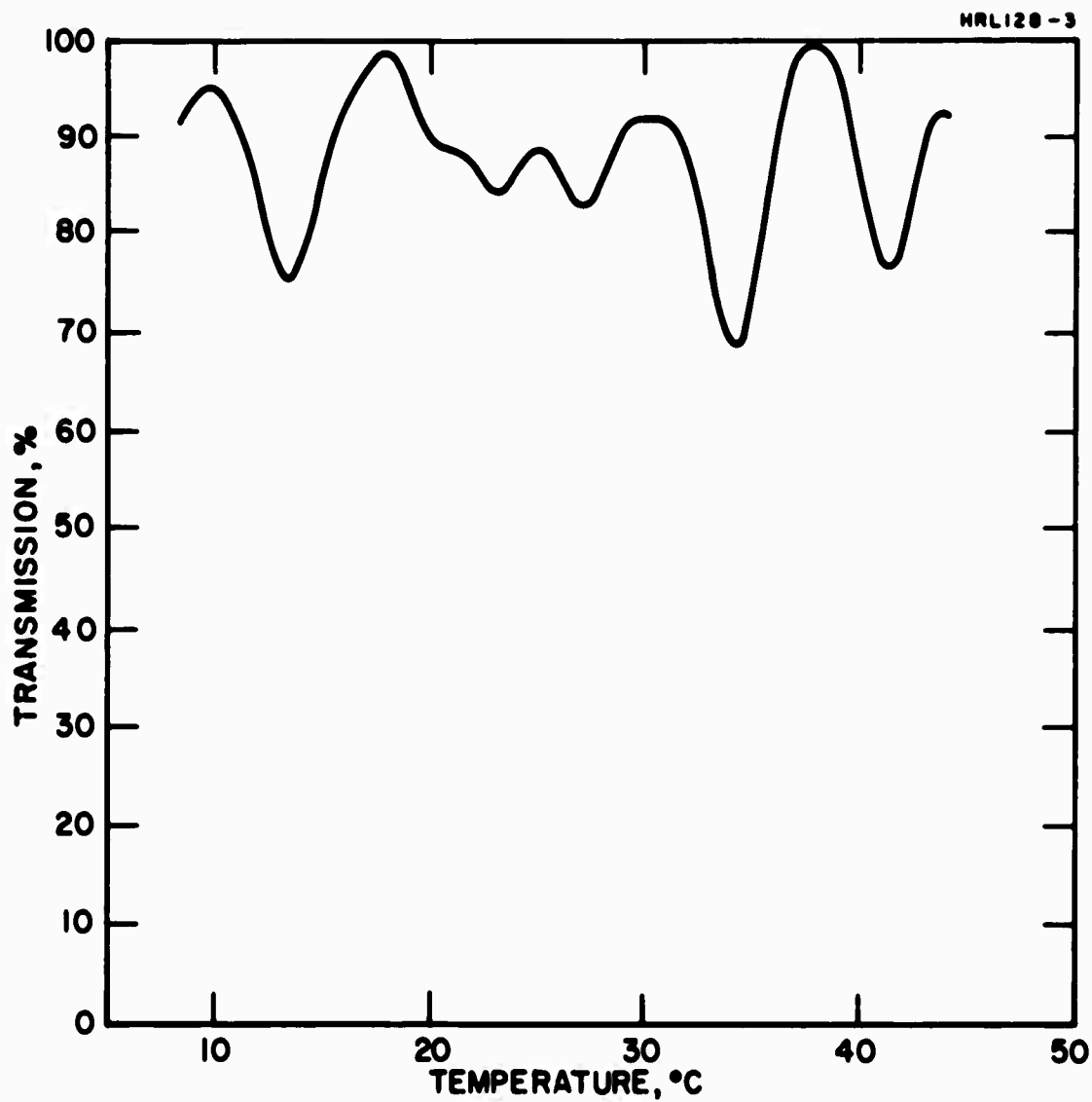


Fig. 7. Plot of percent transmission at 6328 \AA of the resonant reflector versus temperature.

At this writing, a set of elements for the resonant reflector is being reworked by the fabricators (Crystal Optics Research), and it is hoped that they will be received, permanently optically contacted, within a few days. If this reworking is successful, we will soon be able to operate the laser as a reliable single mode device.

D. Results of Threshold Experiments

Early in the program we had the use of a mode controlled giant pulse laser to carry out a few preliminary damage threshold experiments. The main purpose of these early threshold experiments was to determine whether an amplifier would be needed to reach damage threshold. We found, in fact, that with the oscillator alone we were not able to damage the ruby sample internally when we focused with a 50 cm focal length lens; however, a small pit was formed at the exit surface of the sample. When a 12-in. ruby laser amplifier was used in conjunction with the oscillator, we were able to generate extensive bulk damage. The amplifier was pumped to give a gain of about 7 dB. An initial damage threshold value for a ruby sample from Union Carbide was reported to be about 3 GW/cm².

Having established the need for an amplifier, we designed and built one. Once the amplifier was operating reasonably well, we were able to obtain a rough comparison of damage threshold between a typical Union Carbide sample and a ruby boule section from Airtron, which was particularly impressive in its excellent optical and scattering properties. The Airtron sample had been on loan to C.M. Stickley of Air Force Cambridge Research Laboratories. Airtron subsequently consented to sell it to Hughes for the damage study. The Airtron sample has a damage threshold of about a factor of two higher than the Union Carbide sample. The measured values are

	Airtron Sample	Union Carbide Sample
Threshold Power Density	18.8 GW/cm ²	9.05 GW/cm ²
Threshold Energy Density	609 J/cm ²	295 J/cm ²

These measurements were made with no attempt to maintain longitudinal mode control, but with good transverse mode control as shown by near- and far-field photographs. (The far-field beam divergence of the laser is typically 0.7 mrad (full angle), as measured in the far-field photographs; the calculated diffraction limited divergence for a gaussian beam of 1 mm radius is ~ 0.5 mrad. $\theta = 2\lambda/\pi w_0$.) The above power and energy densities were calculated using the assumption that the beam radius is the same at the output of the amplifier as at the input (i.e., 1 mm). The beam radius at the minimum was taken to be 1.1×10^{-2} cm, which is the number calculated according to the method described in the next section. The energy density was calculated using the peak power times the pulse width (32.5 nsec). The power monitors were calibrated against a calibrated Korad biplanar photodiode and calorimeter.

E. Definition of Threshold

The above comparison of damage thresholds for the different samples must be taken as tentative because the definition of damage threshold is somewhat arbitrary. The data which led to that particular set of numbers yield the following observations:

Sample*	Power Density at Focus, GW/cm ²	Remarks
(4) Airtron boule	7.21	No damage
(2) Airtron boule	7.45	Surface pitting
(5) Airtron boule	18.8	2 internal pits
(3) Airtron boule	36.9	Extensive internal damage
(6) Union Carbide Rod	9.05	1 internal pit
(1) Union Carbide Rod	39.3	Extensive internal damage

*The numbers in this column refer to the order of laser shots. The sample was moved so that a different region was exposed for each shot. After each shot the sample was examined by illuminating with a He-Ne laser aligned to the same direction of propagation as the ruby laser.

Shots 5 and 6 were taken to be threshold in that a very small amount of internal damage is observed, but the reproducibility of this observation is not yet known. In addition, the difference in power required to give one or two internal pits, although believed to be insignificant, is not really known. We present these data to point out the tentative nature of the reported threshold numbers. It would be more realistic to state that the damage threshold for the Airtron boule lies between 7 and 19 GW/cm² and that for the Union Carbide rod is 9 GW/cm² or less. We also wish to point out that the surface damage at the exit surface occurs at appreciably lower power than the internal damage; no special surface cleaning techniques were used, however.

In a series of experiments during the exploration of the damaging capability of our amplifier-oscillator combination, we placed a piece of exposed film a few centimeters beyond the ruby sample to observe burn patterns. When extensive bulk damage occurred, the burn spot was about twice as large as that resulting when there was no damage or just surface damage. This probably results from the increased scattering of the laser light by the damage sites. The effect of increasing the angle of forward scattered light has been reported previously.² The fact that the damage is formed during the giant pulse is also substantiated by other workers,³ as well as by some of our early results⁴ where we used an STL camera to photograph the damage in glass while it was being formed.

F. Electron Microscope Observations

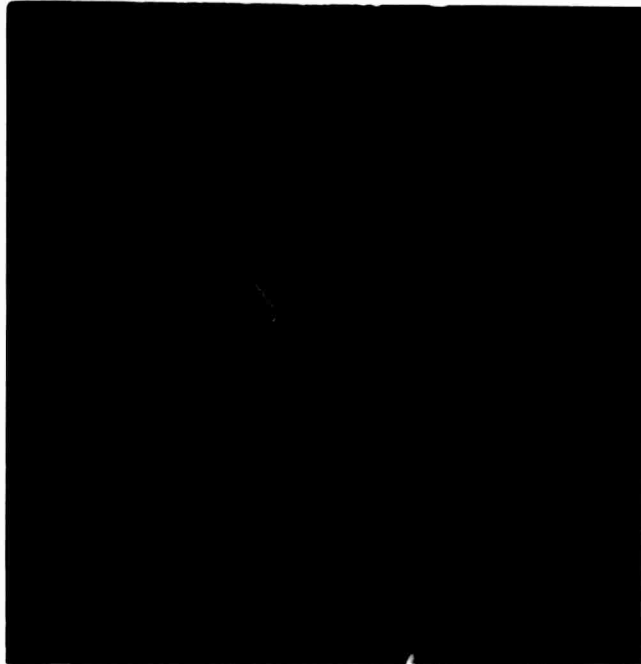
We have used a scanning electron microscope to examine the damage pits formed at the exit surface of a ruby sample. The particular sample is a 1/4 in. diameter x 3 in. long rod from Union Carbide. Figure 8 shows several views of the surface damage under different magnifications. The first picture (Fig. 8(a)) shows the rod under 23x magnification. The damaged areas were caused by three different shots of the laser; the one small pit at the lower left was caused by one shot, the cluster at the lower right by another, and the large craters at the top by a third. Further magnification of the last two regions is seen in the other electron micrographs in the figure. Figures 8(c) and (d) show the large crater at the top magnified 610x and 7000x, respectively. Figures 8(e) and (f) show one of the multiple pits on the lower right magnified 660x and 6600x, respectively. Electron micrographs of the undamaged surface at 7000x magnification show

MRL 120-4



(a) End of ruby rod
at 23x.

M 6969



(b) Undamaged surface
at 7000x.

Fig. 8. Scanning electron micrographs of the exit surface
damage at different magnifications.

M 6770



(c) Region A at 610x.

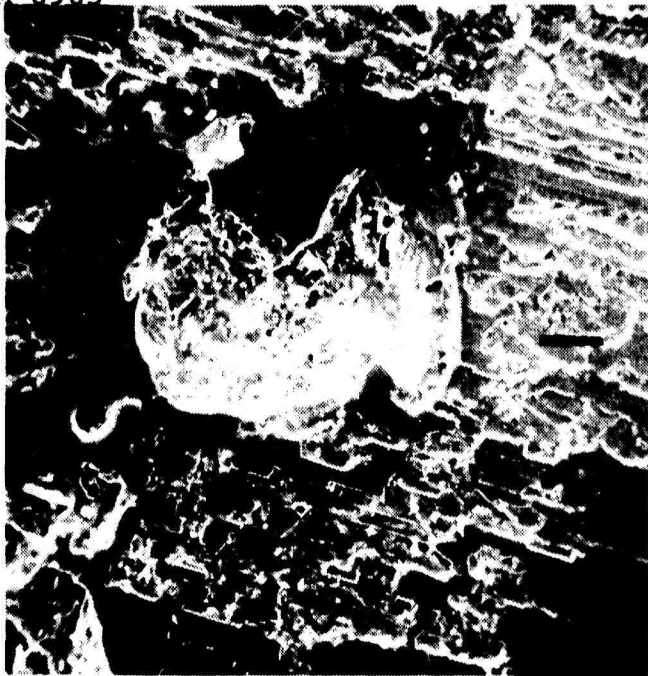
M 6966



(d) Region A at 7000x.

Fig. 8 continued.

M 6965



(e) Region B at 660x.

M 6971



(f) Region B at 6600x.

Fig. 8 continued.

essentially a smooth surface (Fig. 8(b)). The magnified view of the large crater in Figs. 8(c) and (d) shows what appears to be a molten region around the hole, whereas the views of the pitted area (Figs. 8(e) and (f)) appear to be more like multiple fractures than a melting phenomenon.

We do not wish to offer any interpretation of the photomicrographs at this time, but merely present them and point out their potential use as a tool for studying laser induced surface damage.

G. Mode Propagation Computations

In order to have a more detailed understanding of the behavior of the light after it propagates away from the laser, we have calculated the beam size as a function of distance from the laser and thence through the lens to the sample.

Our interest in pursuing these considerations was to answer the following questions concerning the propagation of the fundamental mode.

1. What is the size of the focused spot obtainable when a sample is placed in the beam?
2. What happens to the location of the focused spot when a sample is placed in the beam?
3. How, if at all, are the spot size and location affected by different positions of the air-sample interface?

For this purpose we have used as a starting point an equation derived by V. Evtuhov⁵ from the theory of Boyd and Gordon.⁶

$$W = \frac{W_i^2(r_i+s)^2 + 4s^2r_i^2}{r_i^2 W_i} \quad (1)$$

$$r = \frac{W_i^2(r_i+s)^2 + 4s^2r_i^2}{W_i^2(r_i+s) + 4sr_i^2} \quad (2)$$

where r is the radius of curvature of the wave front, r_i is the initial radius of curvature, s is the distance, and W is related to the beam radius by the relation $W = (2\pi/\lambda) w^2$; w is the beam radius defined as the radial distance for which the field reaches $1/e$ of its peak value (or the $1/e^2$ point for the intensity). W_i is the value of W at the origin or input. If we have a gaussian mode propagating in the s direction starting from a plane through $s = 0$, having an initial radius of curvature r_i and beam radius w_i , eqs. (1) and (2) give the value of W and r at any distance s from the input. When an optical element such as a lens, mirror, or dielectric is placed in the beam, we use the values of W and r at that point as representing new initial conditions for finding further values. For our calculation, therefore, we start at the laser output mirror with a certain initial beam size and radius of curvature ($w_i = 0.1$ cm, $r_i = \infty$) and allow the gaussian wave to propagate to the lens a distance s (1 m in this case) away. Using (1) and (2) we compute the value of r and W at the input to the lens. At the output of the lens W is unchanged, whereas r takes on a new value, $r_{out} = fr_{in}/(f-r_{in})$. These are used as new initial conditions for the propagation of the wave after the lens. (Note that for a plane wave incident on the lens ($r_{in} = \infty$) the outgoing radius of curvature $r_{out} = -f$.) When a material of dielectric constant n is placed somewhere after the lens it is again necessary to compute r and W at this point and use these as new initial conditions. In this case the beam radius w is not changed at the boundary, but the radius of curvature increases by a factor equal to the refractive index n of the medium. (More precisely, the radius of curvature is multiplied by the ratio of refractive indices of the two media.)

Let us define the following unitless quantities:

$$\Omega = \frac{W}{W_i}, \quad \Sigma = \frac{s}{r_i}, \quad \rho = \frac{r_i}{r}, \quad \Lambda = \frac{r}{r_i}$$

Equations (1) and (2) can be rewritten in the following more convenient forms:

$$\Omega = (1 + \Sigma)^2 + 4\Sigma^2\rho^2 \quad (3)$$

$$\Lambda = \frac{(1 + \Sigma)^2 + 4\Sigma^2\rho^2}{1 + \Sigma + 4\Sigma\rho^2} \quad (4)$$

The condition for minimum beam radius can be found by taking the derivative of (3) with respect to Σ or setting the denominator of (4) equal to zero. In either case, one obtains

$$\Sigma(\Omega_{\min}) = \frac{-1}{1+4\rho^2} .$$

Further substitution into (3) gives

$$\Omega_{\min} = \frac{4\rho^2}{1+4\rho^2} .$$

Let us now place in the path a semi-infinite sample of refractive index n . For our purposes we will assume that the light is traveling from left to right. The sample is located such that the air-sample interface is found at an arbitrary distance b from the lens. To the right of boundary b (i.e., inside the material), we will denote the parameters as primed, e.g., Σ' , ρ' , etc. To the left, the variables are unprimed.

At the boundary, we determine new initial conditions for the further propagation of the wave. The radius of curvature just inside the boundary, $f'_b = nr_b$, where r_b is the radius of curvature just outside the boundary. Similarly, $w'_b = w_b$, $n\lambda' = \lambda$; hence, $W'_b = nW_b$.

We now set up new initial conditions at the boundary plane b under two conditions: (1) with sample present, (2) without sample.

The minimum conditions for Case 1 are

$$\Sigma'(\Omega'_{\min}) = \frac{S'_{\min}}{r'_b} = \frac{-1}{1+4\rho_b'^2}$$

$$\Omega'_{\min} = \frac{4\rho_b'^2}{1+4\rho_b'^2}$$

where

$$\rho'_b = \frac{r'_b}{W'_b} = \frac{r_b}{W_b} = \rho_b .$$

The conditions for Case 2 are the same, except that we use the unprimed values corresponding to initial conditions infinitesimally to the left of the boundary.

We see that the value of Ω at the minimum depends solely on the value of ρ which is the same on either side of the boundary. Thus, the size of the focused spot is the same regardless of whether a sample is present, and is independent of the location of the air-sample boundary.

Similarly, the values for Σ are the same but the distance of the minimum from the boundary is different in the two cases.

For Case 1

$$s'_{\min} = \frac{-r'_b}{1+4\rho_b^2} = \frac{-nr_b}{1+4\rho_b^2}$$

For Case 2

$$s_{\min} = \frac{-r_b}{1+4\rho_b^2} .$$

Hence $s'_{\min} = ns_{\min}$. That is, the distance from the plane b to the focus is n times farther when a sample is present than with no sample present.

We summarize the results of the preceding considerations in the following way.* (1) The size of the beam waist of a focused beam is unchanged when any material is placed in the

* We wish to acknowledge the comments of E.S. Bliss, who pointed out an error in an earlier treatment which led to appreciably different conclusions from those we now reach.

path. (2) The location of the beam waist is moved "downstream" n times farther from the sample boundary than it would have been if the sample had not been present.

H. Plans for Next Period

Threshold measurements will be carried out under a variety of different conditions as soon as the resonant reflector can be installed. The parameters which will be varied in the beginning will be sample length, beam size (i.e., focal length of focusing lens), and external pumping. The last may be especially important if photoconductivity is an important factor in the damage mechanism. Samples from different sources will be subjected to test as soon as they become available. Among these will be TiO_2 doped ruby and sapphire from Djeva, which showed a considerably higher damage threshold than undoped material in previous work.'

BLANK PAGE

II. THEORETICAL STUDIES ON OPTICAL DAMAGE

A. Introduction and Summary of Results

During this reporting period our main theoretical efforts have concentrated on the effects of strong optical fields on relatively low densities ($\sim 10^{15} \text{ cm}^{-3}$) of electrons in the conduction band of a transparent polar crystal (with special attention to ruby and sapphire crystals). Various experimenters have presented evidence that electron densities of at least 10^{15} cm^{-3} are photoexcited in ruby and sapphire by optical intensities of the order of 10^{10} W/cm^2 , which are just below damage levels.⁸⁻¹⁰ Previous workers^{1, 11-14} have suggested that at a certain threshold of optical pulse power, these electrons become hot enough to ionize their surroundings and produce a catastrophic electron avalanche that parallels the electron avalanche process long known and studied in dc dielectric breakdown.¹⁵ Our own studies have led us to agree with the general opinion that these electrons are a key link in the optical-pulse damage process, and we agree with all previous workers that the model "polaron" Hamiltonian constructed by Fröhlich to describe the electron-lattice coupling should give at least a good qualitative description of these nondegenerate conduction electrons. However, our studies of electron heating using the lowest order (in coupling and optical intensity) results of the Fröhlich model do not indicate that significant electron heating above ambient lattice temperatures should occur at the optical intensities ($\sim 10^{10} \text{ W/cm}^2$) in question. Furthermore, we find that if these lowest order terms give an adequate description, an entirely new role of the electrons in damage is suggested: the electrons cause the optical energy to be passed to the longitudinal-optical (LO) phonon modes rapidly enough that the subsequent decay of these LO phonons into acoustic phonons (in $\sim 10^{-11}$ sec) sets up acoustic shock waves that result in lattice rupture. We have not yet studied the problem of whether these damage-mediating electrons are created by single- or multiphoton excitation, or possibly by photoemission from inclusions. The photoconductivity that Hochuli⁸ observed in ruby and sapphire was linear in the optical intensity I , so that it occurred presumably by single-photon excitation from impurity levels (a presumption supported by the observed temperature dependence⁸). However, the photoconductivity observed in ruby by Dneprovskii, et al.,⁹ at much higher intensities varied as I^3 . In either eventuality it would appear that the conduction electrons are

being drawn from impurity levels. Therefore, if the new picture of the damage process which we discuss below is valid, there is real hope of raising the damage threshold of a crystal by adding impurities which bind the existing impurity electrons more tightly and reduce the supply of photoelectrons. This possibility does not exist if electron avalanche is important, because avalanche processes occur quite independently of the number of electrons available initially to start the avalanche.

B. Estimate of the Conditions for Crystal Rupture

If the role of the electrons is as we have suggested, their presence results essentially in a certain thermal (heat) energy (which we calculate in the next section) being deposited in the lattice by an optical pulse. To estimate an upper limit on how much energy is required to rupture the crystal, we use the observations of Belikova and Sviridenkov¹⁰ of the damaging shock waves that formed at breakdown around a focal region $\sim 10^{-1}$ cm long and $\sim 10^{-2}$ cm wide. By measuring the shock velocity, they estimated that the shock energy ($\sim 10^{-1}$ J) was essentially the same as the energy that was observed to be absorbed and scattered from the 0.3 - 0.5 J, 10^{-8} sec optical pulse. (They estimated that this energy corresponded to shock front pressures of the order of the yield stress in ruby, 10^5 psi.) Therefore, we may estimate that when the photoexcited electrons produce an optical absorption coefficient κ cm⁻¹ of order unity, damage will certainly result. Other observations of our own and others³ have indicated that in fact damage may occur with less than 10% absorption from the beam; we believe that for some beam geometries (as yet uncertain), as little absorption as $\kappa \sim 10^{-1}$ to 10^{-2} is sufficient to initiate a damaging acoustic shock.

Unfortunately, to date there are no calculations of how the damaging shock is formed from the temperature and pressure gradients caused by the deposited energy, so that we have no good theoretical corroboration of these numbers. However, we have been able to estimate from standard hydrodynamic theory that the threshold for stimulated thermal Rayleigh scattering from a 10^{10} W/cm² beam occurs in ruby when $\kappa \sim 1$. In the next section we show from polaron theory that it requires on the order of 10^{16} electrons/cm³ in a ruby or sapphire to produce an absorption coefficient of order 10^{-1} cm⁻¹, a figure which is consistent with our idea that the photoelectrons can damage by mediating lattice heating without ionizing the lattice.

C. Calculation of Heating and Absorption by Conduction Electrons

Fröhlich's model Hamiltonian H for a photoexcited electron coupled to its surrounding lattice and in an oscillating x-directed electric field $E(t)$ is

$$H = h + u + v \quad (5)$$

where

$$h = p^2/2 + \sum_k \omega_k a_k^\dagger a_k \quad (6)$$

describes the uncoupled electron (of momentum p) and free longitudinal polar lattice modes of frequency ω_k (whose annihilation operators are a_k). Here

$$u = \sum_k C_k a_k \exp(ik \cdot x) + \text{h.c.} \quad (7)$$

describes the electron-lattice coupling; and

$$v = -xE(t) \quad (8)$$

describes sufficiently accurately the coupling of the electron with position coordinate x to the optical field. We employ polaron units, unless otherwise stated, where $\hbar = m^* = 1$, and m^* is the electron's (assumed parabolic) band mass for a stationary lattice. Fröhlich derived the coupling coefficient values $C_k = 2^{3/4} \pi^{1/2} \alpha^{1/2} / k$ where the dimensionless measure α of the electron lattice coupling strength is defined by

$$\alpha = (\epsilon^{-1} - \epsilon_0^{-1}) (\hbar\omega/\text{Ryd})^{-1/2} \quad (9)$$

and ϵ_0 , ϵ are the dc and optical dielectric constants of the crystal. The longitudinal optical phonon frequency is approximated by the constant ω and Ryd is the Rydberg constant for an electron of mass m^* .

If the coupling constant α is not large compared with unity, calculated quantities may be developed in a perturbation series in α . The terms of order α^0 or α generally give fairly accurate predictions, even for α 's as large as unity. For ruby or sapphire, $\epsilon \sim 3$, $\epsilon_0 \sim 9$, but the effective band mass is unknown. If we take the band mass to be the free electron mass and take $\hbar\omega =$ Boltzmann's constant k times the Debye temperature (980°K), then (5) gives $\alpha \sim 3$, which is unfortunately too large for a weak coupling approximation to be accurate. To examine the electron energy gain, however, we will proceed as if α were small (as did all previous theories of damage), with the knowledge that methods are available to calculate this more accurately,¹⁶ as we are attempting at present.

First, to determine whether the electron does heat up appreciably, we have assumed that the optical field was turned on at $t = 0$ and calculated the expected kinetic energy $K = 1/2 \langle \dot{x}^2(t) \rangle$ of the electron at later times t using (1). We have found that

$$2K = kT + V^2(t) [1 + O_1(\alpha) + O_2(E^2/E_0^2)] \quad (10)$$

where T is the local lattice temperature and $V(t)$ is the expected velocity of an electron initially at rest and driven by the electric field $E(t)$ in the presence of lattice damping. The corrections O_1 and O_2 are of order α and $(E/E_0)^2$ where E_0 is a characteristic electric field

$$E_0 = (\omega^2/e) (\hbar m^*/\omega)^{1/2} \text{ esu} \quad (11)$$

where e is the electric charge in esu. For $E > E_0$ the electron develops large coherent nonlinear response. This field is seen to be on the order of 10^5 to 10^6 V/cm for ruby, and corresponds to optical power densities of the order of damage threshold densities. (Our calculations of these nonlinear corrections indicate they do not qualitatively affect the damage process, but tend to decouple the electron from the lattice. We will neglect them here.) The important characteristic of all the terms in (6) for the expected kinetic energy is that, after a brief and small transient, the kinetic energy becomes essentially constant in time in an optical field of constant amplitude. This is in contrast to the

suggestions of all previous workers^{3,11-14} that in these circumstances the electron might continually gain energy in time until it had enough energy (~ 10 eV) to ionize, as it might indeed gain in a dc electric field.¹⁵ Because no previous worker has calculated $K(t)$ and examined this point, we cannot point to any calculational error that might have led them to suppose that the optical damage would imitate dc dielectric breakdown in that very hot electrons would be created.

It is easy to estimate that, since (as we will show) the electron-to-lattice damping rate is small compared with the optical frequency ν , $V(t) \sim E(t)/\nu^2$ so that $\langle V^2 \rangle$ is of the order of 10^{-5} eV when E is near the damage level. Therefore, to the lowest orders of approximation the average electron kinetic energy is always close to the thermal energy ($\sim 1/40$ to $1/4$ eV) that it would have in equilibrium with the lattice in its vicinity. Finding this result, we proceeded to calculate, using (5), the expected rate of increase in the total phonon energy to lowest order in α . We found, as expected, that the phonon energy does increase proportionally with time (in a constant optical field) with a rate that matches the rate calculated by others¹⁴ at which the electric field does work on the electron.

This confirms the idea that the electrons nearly instantly pass all the energy that they receive from the field on to the optical phonons. We have not yet been able to confirm that the field-to-electron energy transfer rate matches the electron-to-lattice rate at arbitrary coupling, temperature, and optical intensity, but the structure of the general equation for K indicates that it is indeed constant in a constant amplitude field, and thus we now believe that the creation of hot electrons when they are coupled only to a cold lattice is improbable. However, a possible complication that we will study further is that a very few electrons might be created in the high energy wings of the electron distribution.

To obtain an estimate of the expected rate γ at which the optical field of amplitude E oscillating at a frequency ν does work on an electron, we may use the polaron response theory derived by Feynman, et al.,¹⁶ using Fröhlich's Hamiltonian

$$\gamma = \frac{1}{2} E^2 \text{Im}[\nu^2 - \chi(\nu)]^{-1} \quad (12)$$

and

$$\text{Im}\chi(\nu) = \frac{2\alpha\pi^{-1/2}\beta^{3/2}\sinh(\beta\nu/2)}{3\sinh(\beta/2)} \left(\frac{\nu}{w}\right)^3 \int_0^\infty \frac{\cos(\nu u) \cos u \, du}{[u^2 + a^2 - b \cos(\nu u)]^{3/2}} \quad (13)$$

We have redefined our units so that the phonon frequency ω is 1 (making $\nu \sim 17$ at the ruby laser frequency), time is expressed in units ω^{-1} , energy in units of $\hbar\omega$, etc. The parameter $\beta = \hbar\omega/kT$ is ~ 3.3 for ruby and sapphire at room temperature. The parameters ν and w are chosen from a variational principle which gives $\nu = 3.4$, $w = 2.55$ for $\alpha = 3$ and in the limit of low temperatures¹⁶; $a^2 \equiv \beta^2/4 + Rb \coth(\beta\nu/2)$; $R \equiv (\nu^2 - w^2)/(w^2\nu)$; and $b \equiv Rb/\sinh(\beta\nu/2)$. With the above parameters $R = 0.229$, $a = 1.866$, and $b = 5.53 \times 10^{-3}$.

The integrand in (13) can be expanded in powers of b and each term integrated to obtain the value of γ . Unfortunately, the series converges rather slowly for the high frequencies of interest, reflecting the fact that the oscillating electron can lose energy by processes in which 1, 2, or many phonons are emitted. We are in the process of evaluating the integral numerically for various parameters. A first estimate of (13) using the above parameters shows $\text{Im}\chi \sim 40$, a value sufficiently accurate for our present qualitative estimates.

The optical beam absorption coefficient κ is simply related to χ by

$$\kappa/k_0 = (\omega_p^2/\epsilon) \text{Im} [\nu^2 - \chi]^{-1} \quad (14)$$

where ω_p is the electron plasma frequency in our units and equals $(4\pi Ne^2/m^*)^{1/2}$ in cgs units, where N is the number density of electrons. To obtain $\kappa \sim 0.1 \text{ cm}^{-1}$ when k_0 , the optical wavevector length in the crystal is $\sim 10^5 \text{ cm}^{-1}$, we would require, according to our above estimates, that ω_p be on the order of 1/30 of the phonon frequency. This corresponds to an electron density of $\sim 10^{16} \text{ cm}^{-3}$ if the effective mass is unity. It is important to note that with $\text{Im}\chi$, there is a real part of χ which will contribute to a nonlinear index and which also has the effect of altering the effective mass of the electron, although probably not by more than a factor of 2.

D. Plans for Next Period

To examine the validity of our new picture of the role of photoexcited electrons in crystal damage, we plan to (a) to try to establish a firm dynamical acoustic theory for the formation of shock waves, given the thermal energy profile deposited by the optical beam; (b) to evaluate precisely the predictions of Fröhlich's polaron model for the damping of the driven optical motions of the electrons; (c) to evaluate the tendency of the electron to gain energy in the form of incoherent motions under the influence of the optical beam; (d) to examine further the various mechanisms of photoexcitation; (e) to calculate the nonlinear index of refraction seen by the optical beam because of the presence of conduction electrons; (f) to calculate the nonlinear effects on the absorption rate that occur at high fields; and (g) to continue to search for possible processes in which these electrons are not important to damage at all.

REFERENCES

1. "Damage Threshold Studies in Laser Crystals," Technical Proposal No. 69M-8949/B8979, Hughes Research Laboratories, March 1969.
2. "Research into the Causes of Laser Damage to Optical Components," Final Report, Contract DA-28-043 AMC 00009, Perkin-Elmer Corporation.
3. T.P. Belikova, A.N. Savchenko, and E.A. Sviridenkov, "Optic breakdown in ruby and related effects," Soviet Phys.-JETP 27, 19-23 (1968).
4. C.R. Giuliano, unpublished work.
5. V. Evtuhov, private communication.
6. G.D. Boyd and J.P. Gordon, "Confocal multimode resonator for millimeter through optical wavelength masers," Bell System Tech. J. 40, 453-488 (1961).
7. G. Nath and G. Walda, "Strong reduction of laser produced damage in sapphire and ruby by doping with TiO_2 ," Z. Naturforsch. 23a, 624-625 (1968).
8. Urs E. Hochuli, "Photoconductivity in ruby and sapphire," Phys. Rev. 133A, 468-471 (1964).
9. V.S. Dneprovskii, D.N. Klyshko, and A.N. Penin, "Photoconductivity of dielectrics under the influence of laser radiation," JETP Letters 3, 251-253 (1966).
10. T.P. Belikova and E.A. Sviridenkov, "Photoconductivity of ruby when strongly irradiated by a ruby laser," JETP Letters 3, 257-259 (1966).
11. A. Wasserman, "A mechanism for damage in solids by intense light," Appl. Phys. Letters 10, 132-133 (1967).
12. V.A. Pashkov and G.M. Zverev, "Destruction of ruby and leucosapphire crystals by strong laser radiation," Soviet Phys.-JETP 24, 516-518 (1967).
13. E.A. Sviridenkov, "Mechanism of damage of ruby by laser radiation," Soviet Phys.-Solid State 9, 1917-1918 (1968).

14. G.M. Zverev, T.N. Mikhailova, V.A. Pashkov, and N.M. Solov'eva, "Mechanisms of destruction of ruby and leucosapphire crystals by powerful laser radiation," Soviet Phys.-JETP 26, 1053-1057 (1968).
15. H. Fröhlich, "Theory of electrical breakdown in ionic crystals," Proc. Phys. Soc. (London) A160, 230-241, (1937).
16. R.P. Feynman, R.W. Hellwarth, C.K. Iddings, and P.M. Platzman, "Mobility of slow electrons in a polar crystal," Phys. Rev. 127, pp. 1004-1017 (1962).

DOCUMENT CONTROL DATA - R&D

(Security classification of title, body of abstract and indexing annotation must be entered when the overall report is classified)

1. ORIGINATING ACTIVITY (Corporate author) Hughes Aircraft Company, Research Labs. Div. 3011 Malibu Canyon Road Malibu, California 90265		2a. REPORT SECURITY CLASSIFICATION Unclassified	
		2b. GROUP	
3. REPORT TITLE DAMAGE THRESHOLD STUDIES IN LASER CRYSTALS			
4. DESCRIPTIVE NOTES (Type of report and inclusive dates) Semiannual Technical Report No. 1,		21 May 1969 through 21 December 1969	
5. AUTHOR(S) (First name, middle initial, last name) Concetto R. Giuliano, Robert W. Hellwarth, LaVerne D. Hess, and Gerald R. Rickel			
6. REPORT DATE January 1970		7a. TOTAL NO. OF PAGES 34	7b. NO. OF REFS 16
8a. CONTRACT OR GRANT NO. F19628-69-C-0277 ARPA Order No. 1434		8a. ORIGINATOR'S REPORT NUMBER(S) Semiannual Report No. 1	
b. PROJECT, TASK, WORK UNIT NOS. 8693-n/a-n/a			
c. DOD ELEMENT 61101D			
d. DOD SUBELEMENT n/a		9b. OTHER REPORT NO(S) (Any other numbers that may be assigned this report) AFCRL-70-0178	
10. DISTRIBUTION STATEMENT This document has been approved for public release and sale; its distribution is unlimited.			
11. SUPPLEMENTARY NOTES This research was supported by Advanced Research Projects Agency		12. SPONSORING MILITARY ACTIVITY Air Force Cambridge Research Laboratories (CRO) L.G. Hanscom Field Bedford, Massachusetts 01930	
13. ABSTRACT In this report a mode-controlled giant pulse laser oscillator and amplifier are described. The oscillator employs a temperature-controlled resonant reflector, a dye Q-switch laser and a 2 mm aperture to assure single mode operation. The result of preliminary threshold measurements on a few different ruby samples are presented. Equations which describe the propagation of the gaussian mode are examined in order to answer some important questions concerning focusing inside dielectric media. The potential usefulness of the scanning electron microscope as a tool for examining surface damage is pointed out by the presentation of a few interesting photomicrographs. The theoretical effort is concentrated on the effects of strong optical fields on relatively low densities of electrons in the conduction band of a transparent polar crystal. The present studies have led to agreement with the general opinion that these electrons are a key link in the optical pulse damage process. However, the present work indicates that significant electron heating above ambient lattice temperatures does not occur at the optical intensities in question. An entirely new role of the electrons in laser induced damage is suggested.			

14.	KEY WORDS	LINK A		LINK B		LINK C	
		ROLE	WT	ROLE	WT	ROLE	WT
	Laser-induced damage Single-mode ruby lasers Gaussian modes Threshold measurements Electron micrographs Theory Conduction electrons Phonon heating						